ISSN 1995-0780, Nanotechnologies in Russia, 2011, Vol. 6, Nos. 3–4, pp. 218–226. © Pleiades Publishing, Ltd., 2011.
Original Russian Text © A.Ya. Neiman, A.V. Tanskaya, E.V. Tsipis, L.M. Fyodorova, B.D. Antonov, 2011, published in Rossiiskie Nanotekhnologii, 2011, Vol. 6, Nos. 3–4.

Effect of Size Factor on Mechanism of Interaction between $A1_2O_3$ and Bi_2O_3 and Conductivity of Composite on Their Basis

A. Ya. Neiman[a], A. V. Tanskaya[a], E. V. Tsipis[b], L. M. Fyodorova[a], and B. D. Antonov[c]

[a] *Ural State University, Yekaterinburg, 620083 Russia*
[b] *Chemistry Department, Instituto Tecnológico e Nuclear, CFMC-UL, EN 10, 2686-953 Sacavém, Portugal*
[c] *Institute of High-Temperature Electrochemistry, Ural Division, Russian Academy of Sciences, Yekaterinburg, 620219 Russia*
e-mail: Arkady.Neiman@usu.ru

Received June 23, 2010; in final form, December 9, 2010

Abstract—The fundamental differences in the mechanism of interaction between nanosized ($Al_2O_3^N$) and microsized ($Al_2O_3^M$) and Bi_2O_3 and routes of charge transfer in the resulting composite consisting of $Bi_2O_3^M$, reaction products, and $Al_2O_3^N$ are shown. The size effect is manifested by a strong adhesion of $Al_2O_3^N$ grains to microsized $Bi_2O_3^M$ grains and by the high reactivity of $Al_2O_3^N$. Both factors result in the encapsulation of $Bi_2O_3^M$ grains in a shell of low-conducting $Al_2O_3^N$ grains and interaction products. The $\alpha \longrightarrow \delta$-$Bi_2O_3$ phase transition at 730°C is registered using the HTXRD and DSC techniques, but it does not appear in the temperature dependence of conductivity because it occurs within mutually isolated $Bi_2O_3^M$ grains. Further heating to 780°C results in the solid-phase decomposition of interaction products and the separation of the δ-Bi_2O_3 phase. Last, a connected charge percolation matrix is formed of highly conducting δ-Bi_2O_3 grains. Due to this, a 2.5-fold conductivity jump is observed in the range of 770–800°C. The above-described model is confirmed by measurements of $\sigma(T)$ for four model cells and by the presence of three concentration ranges for the $[Al_2O_3^N]/[Bi_2O_3^M]$ ratio, which have different shapes of the $\sigma(T)$ dependence and different locations of the σ jump in the range of 730–805°C.

DOI: 10.1134/S1995078011020133

INTRODUCTION

The great prospects for the practical application of nanooxide-based materials imply the presence of an adequate database on the regularities of reactivity and the specific character of the mechanism of solid-phase transformations with their participation [1]. However, these problems have not been studied in practice despite their fundamental and practical importance: the direct relationship to the problem of thermodynamic and kinetic stability that both nanostructured substances and functional nanotechnological devices have.

It would be natural to expect that this gap would have been filled recently as a result of intensive research into nanosized systems and materials.

One example of a particular manifestation of the structural and thermodynamic changes in a substance in a nanosized form is the phase size effect. Thus, in nanocomposites, high-temperature phases are stabilized and the spontaneous dispersion of components and their amorphization occur [2, 3].

At minimum, a strong interfacial interaction results in the formation of nonautonomous phases distributed along the interface surface that are fundamentally different from interfacial phases in regards to their structure and properties. One example of this is the formation of a nonautonomous $Me\mathrm{W}_{-S}$ phase at the $Me\mathrm{WO}_4$ | WO_3 contact (Me = Ca, Sr, Ba) [4–6]. The MeW_{-S} phase is characterized by high ionic conductivity. As a result, $\{\mathrm{MeWO}_4 \cdot x\mathrm{WO}_3\}$ composites feature electrolytic ionic conductivity, which distinguishes them fundamentally both from MeWO_4 (a high–temperature insulator) and WO_3 (an n-type semiconductor). To identify composites of this type, the terms "*meta*-composites" and "*meta*composite ionic conductivity" were suggested [4–6].

As was pointed out above, data on the reactivity of nanooxides and the mechanism of synthesis reactions upon their participation are practically absent in the

literature. At the same time, several nontrivial facts were described in the recent work [7]. Here, in particular, the reactions of $NiO^{M,N} + MoO_3^M$, $Al_2O_3^{M,N} + Bi_2O_3^M$ and $NiO^{M,N} + Al_2O_3^{M,N}$ were studied (indices M and N denote micro- and nanosized oxides, accordingly). The results showed that the manifestation of the nanofactor depends on the nature of partner oxides, particularly on the character and metal–oxygen bonding energy; the value and ratio of the surface energy; the ability of a more "active" oxide to disperse; surface (at the *solid|gas* interface) and interfacial (at the *solid A|solid B* interface) mobility; temperature and oxygen activity in the gas phase; and, finally, on the experimental conditions (the contact sintering of ceramic disks or the interaction in a powder mixture). Thus, the diffusion penetrability of the $NiMoO_4$ layer formed on the NiO^N surface turned to be twice as low as that of the layer formed on the NiO^M surface. The solid-phase spreading (dispersion) of NiO^M in contact with $Al_2O_3^N$ is found starting at relatively low temperatures.

However, the following effect was of most interest: the temperature dependence of conductivity (heating to 760°C) of the $Al_2O_3^N + Bi_2O_3^M$ equimolar mixture featured no conductivity jump by 3 orders of magnitude related to the known α-$Bi_2O_3 \longrightarrow \delta$-$Bi_2O_3$ modification transition (the equilibrium transition temperature was ≈730°C [8, 9]). At the same time, the conductivity jump was registered at the due temperature in the course of heating the $Al_2O_3^M + Bi_2O_3^M$ mixture. This fact was interpreted as a result of the stabilization of the low-temperature α-Bi_2O_3 form as a result of the interfacial interaction with $Al_2O_3^N$. However, the nature and mechanism of the stabilization effect remained unclear.

Accordingly, the key goal of this study was to research the nature and mechanism of the reaction and transport processes occurring at the $Bi_2O_3^M$ | $Al_2O_3^N$ interface.

Al_2O_3 | Bi_2O_3 SYSTEM; PHASE REACTIONS AND PROPERTIES

In the subsolidus region of the Al_2O_3 | Bi_2O_3 system, complex compounds exist with the following ratio of $Al_2O_3 : Bi_2O_3$ [8, 9]:

$$Al_2Bi_{24}O_{39}\ (1:12)\ \text{decomposes at } 755^\circ C \quad (Al_2Bi_{24}O_{39} \longrightarrow 2BiAlO_3 + 11\delta\text{-}Bi_2O_3), \tag{1}$$

$$BiAlO_3\ (1:1)\ \text{decomposes at } 800^\circ C \quad (4BiAlO_3 \longrightarrow Al_4Bi_2O_9 + \delta\text{-}Bi_2O_3), \tag{2}$$

$$Al_4Bi_2O_9\ (2:1)\ \text{melted incongruently at } 1070^\circ C \quad (Al_4Bi_2O_9 \longrightarrow Al_2O_3 + L). \tag{3}$$

The eutectic between $Al_2Bi_{24}O_{39}$ and δ-Bi_2O_3 corresponds to 820°C. Bi_2O_3 melts at 825°C.

The surface energy of Bi_2O_3 (20×10^{-6} J/cm^2), though low in itself, is several times lower than that of Al_2O_3 (90×10^{-6} J/cm^2) [10], which is why Bi_2O_3 is easily dispersed and spread over the surface of Al_2O_3 [11], providing the extension of the reaction zone and the uniform accessibility of the partner oxide for the occurrence of various transitions. Therefore, the solid-phase chemical interaction between Bi_2O_3 and Al_2O_3 occurs on the basis of the diffusion transport of components of Bi_2O_3 through the reaction products in the direction of Al_2O_3 ($Bi_2O_3 \longrightarrow Al_2O_3$) and includes a number of serial-parallel charge transitions [8, 11],

$$Bi_2O_3 + 12Al_2O_3 \longrightarrow Al_2Bi_{24}O_{39}, \tag{4}$$

$$Al_2Bi_{24}O_{39} + 11Al_2O_3 \longrightarrow 24BiAlO_3, \tag{5}$$

$$2BiAlO_3 + Al_2O_3 \longrightarrow Al_4Bi_2O_9, \tag{6}$$

occurring in a wide temperature range. The above transitions are complicated by mutual transitions of several modifications of Bi_2O_3 [8, 9].

Two thermodynamically stable modifications are distinguished between Bi_2O_3 polymorphic modifications: an α form that reconstructs under heating to 730 ± 5°C with a transition to the high-temperature δ form. The latter has a fluorite structure with 1/4 of unfilled sites in an O^{2-} sublattice. The $\alpha \longrightarrow \delta$ transition of Bi_2O_3 is accompanied by a conductivity jump of 3 orders of magnitude. The conductivity of the δ form is purely ionic and a current all-time high for solid electrolytes with a conductivity by O^{2-} [12, 13]. It is this property that makes it possible to sometimes identify microscopic amounts of Bi_2O_3 in multiphase systems to an accuracy above that of the conventional XRD technique.

INITIAL SUBSTANCES AND TECHNIQUES

Powder of nano-Al_2O_3 ($Al_2O_3^N$) was used in this paper. It was obtained by the "dry" technique: the electric blasting of Al wire in an oxidative atmosphere [14]. One specific feature of this composition is the absence of aqueous-organic precursors and intermediates at all synthesis stages. This eliminates the problem of taking into account the topochemical memory of the material and makes it possible to potentially study the reactivity nanoaspects. For comparative experiments, $Al_2O_3^N$ obtained by the decomposition of pseudoboehmite ($2AlOOH \longrightarrow Al_2O_3^N + H_2O$) at 550°C for 4 h was used. Microsized $Bi_2O_3^N$ powder (Reakhim) was of reagent grade.

A particle size of $Al_2O_3^N$ was assessed on the basis of the data of electronic microscopy, SEM (the LEO-982

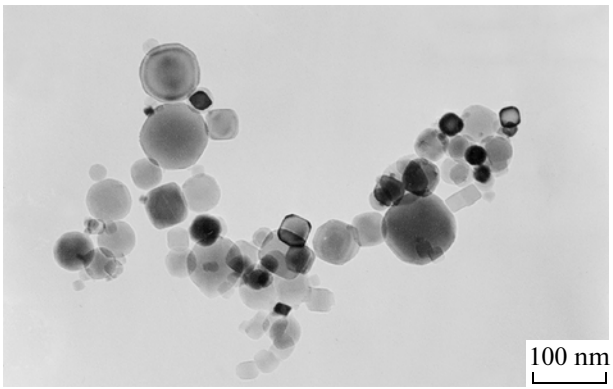

Fig. 1. Bright-field TEM image of the $Al_2O_3^N$ nanopowder obtained using the electric blasting technique.

device), and TEM (the JEM-200 device). Figure 1 shows a bright-field TEM image of $Al_2O_3^N$. The particle size for $Al_2O_3^N$ and $Bi_2O_3^N$ was determined using an Olimpus optical microscope. S_{sp} was determined according to the BET technique (using a 93.5% He–6.5% Ar mixture). The size characteristics of the powders used are presented in Table 1. According to the XRD data (DRON-3M; CoK_α-radiation), $Al_2O_3^N$ was two-phase and contained approximately similar amounts of γ- and δ-modifications of Al_2O_3.

The electric resistance of powdered briquette mixtures was measured using the double-contact ac technique with an R-5030 RLC-meter ($f < 10^5$ Hz). All nonisothermal experiments with mixture-resistance measurements were performed at the heating–cooling rate of 5 or 10 K/min. Individual nano- and microsized oxides and their mixtures were treated in a UZDN sonifier (10 kHz, 1 h) in a medium of dehydrated isopropanol and then uniaxially compacted into disks (∅10 × 2 mm) under the pressure of 2000 kg/cm^2. Let us note that the concentration in mol % in the $Bi_2O_3 | Al_2O_3$ system was close to the concentration in vol %.

High-temperature X-ray phase analysis was carried out using a RIGAKU D/MAX Ultima III diffractometer in Cu$K\alpha$ radiation with λ = 1.54056 Å. Measurements were carried out in the range of 0.02°C at a rate of 4 deg/min. A differential scanning calorimetry analysis was performed using the STA 409 PC Luxx device (NETZSCH) integrated with a QMS 403 CF Aelos quadrupole mass spectrometer of the same company. The measurements were performed in the heating–cooling mode at a rate of 10 deg/min.

EXPERIMENTAL DATA

Conductivity

At the first stage, conductivity measurements were performed for "raw" (compacted but not presintered) oxide mixtures. Experiments in [7] were performed under heating to a temperature of 760°C. In this paper the maximum heating temperature was higher, but it did not exceed 805°C (heating was limited by the proximity of the eutectic horizontal of the $Bi_2O_3 | Al_2O_3$ system (820°C) and the T_{melt} of Bi_2O_3 (825°C) [8, 9]).

Figure 2 shows the temperature dependence of conductivity for a Bi_2O_3 briquette in the heating–cooling mode. It may be seen that, in accordance with the literature data, a drastic conductivity jump occurs at 730°C (a transition from the α to δ Bi_2O_3 modification). The same figure also shows the temperature dependence of the conductivity of the $Al_2O_3^N$ briquette with the value being several orders of magnitude lower.

As opposed to pure Bi_2O_3, a different pattern was always observed in the measurements of conductivity for (1 : 1) mixtures of $Al_2O_3^N$ of different dispersion degrees (S_{sp} = 36.7, 91.4, 97.5, and 113.5 m^2/g) with the $Bi_2O_3^M$ oxide (Fig. 3). The conductivity jump started with a weak step (inflection) at ≈735°C, but the largest part of the jump started at ≈765°C and ended at ≈795°C; i.e., compared to individual bismuth

Table 1. Size characteristics of the applied oxides

Sample no.	Oxide	S_{sp}, m^2/g	Average particle size, nm
1	α-$Al_2O_3^M$ (reactive)	0.13	1.3×10^4
2	$Al_2O_3^N$	36.7	46
3	$Al_2O_3^N$	91.4	35
4	$Al_2O_3^N$	97.5	20
5	$Al_2O_3^N$	113.5	18
6	$Al_2O_3^N$ (obtained by sintering pseudoboehmite)	95.0	25
7	α-$Al_2O_3^M$, obtained by sintering $Al_2O_3^N$	–	1.0×10^4
8	$Bi_2O_3^M$, reactive	–	8×10^3

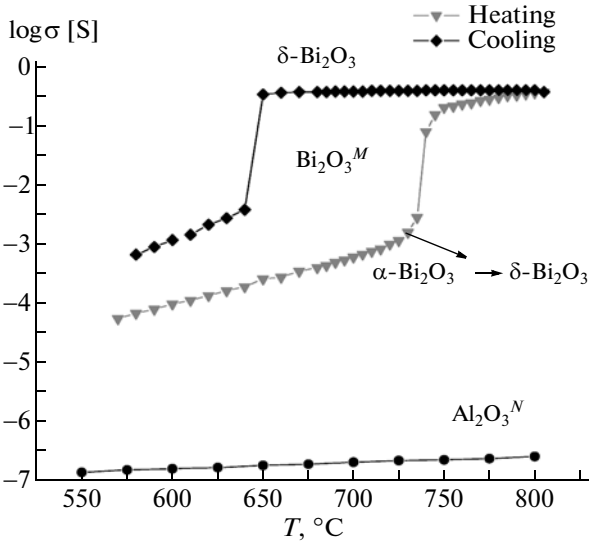

Fig. 2. Temperature dependence of the conductivity of ceramics of individual $Bi_2O_3^M$ and $Al_2O_3^N$ oxides.

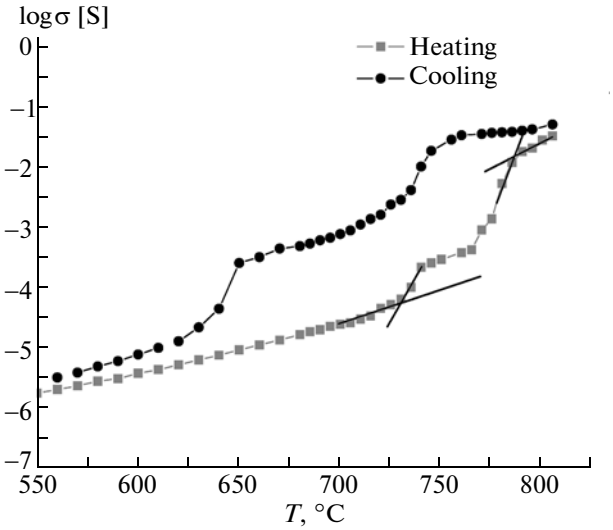

Fig. 3. Temperature dependence of the conductivity of a briquette of the $\{Al_2O_3^N \cdot Bi_2O_3^M\}$ equimolar mixture prepared on the basis of $Al_2O_3^N$ (S_{sp} = 97.5 m^2/g).

oxide, the jump shifted towards higher temperatures and its shape changed. Let us note that the overall height of the conductivity jump observed for the mixtures was 2.5 orders of magnitude; this is the same as in the case of single-phase Bi_2O_3 (Fig. 2).

There is another significant difference appearing in the curves of cooling of the $\{Al_2O_3^N \cdot Bi_2O_3^M\}$ and $Bi_2O_3^M$ mixtures: the lower limit of the temperature range of the hysteresis region corresponding to the kinetic stability of the δ-Bi_2O_3 phase is significantly narrowed. It does not appear below 730°C for any composition with $Al_2O_3^N$ with various dispersion degrees (Fig. 3), while in the case of $Bi_2O_3^M$ it is near 650°C (Fig. 2). It is of importance that the σ(*T*) dependence of the $\{Al_2O_3^N \cdot Bi_2O_3^M\}$ mixtures remained practically unchanged even after 10 heating ⟷ cooling successive cycles (Fig. 4).

At the same time, in a mixture made of a reactive α-$Al_2O_3^M$ sample (Table 1, sample 1), a conductivity jump was registered at the temperature of ≈730°C, which is characteristic of $Bi_2O_3^M$ (Fig. 5).

In connection with this, a control experiment was performed using the $\{Al_2O_3^M \cdot Bi_2O_3^M\}$ mixture, but $Al_2O_3^M$ was prepared on the basis of $Al_2O_3^N$ (Table 1, sample 5) by sintering for 4 h at 1200°C (full transition of γ-, δ-$Al_2O_3^N$ into α-$Al_2O_3^M$ with a particle size of ≈10 μm was confirmed using the XRD technique). The σ(*T*)-dependence for the given control mixture agrees well with the σ(*T*) data presented in Figs. 2 and 5: a conductivity jump also occurred at ≈730°C.

Thus, it was found that screening of the α ⟶ δ-Bi_2O_3 transition in the σ(*T*)-dependences of the $\{Bi_2O_3^M \cdot Al_2O_3^N\}$ mixtures is related to the very presence of nanosized $Al_2O_3^N$.

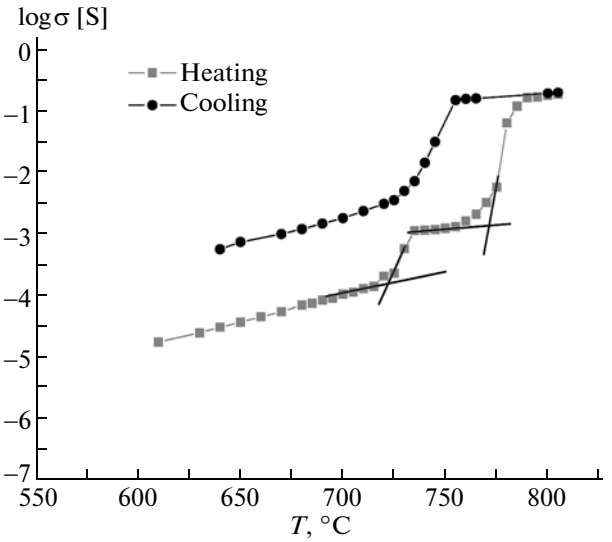

Fig. 4. Temperature dependence of conductivity of a briquette of the $\{Al_2O_3^N \cdot Bi_2O_3^M\}$ equimolar mixture prepared on the basis of $Al_2O_3^N$ (S_{sp} = 97.5 m^2/g) (the tenth heating ⟷ cooling cycle).

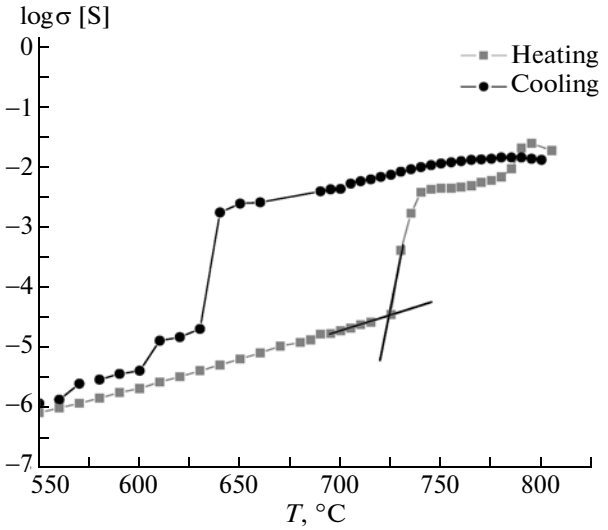

Fig. 5. Temperature dependence of the conductivity of a briquette of the $\{Al_2O_3^M \cdot Bi_2O_3^M\}$ equimolar mixture prepared on the basis of microsized Al_2O_3 (Table 1, sample 1).

At a further stage in this work, the $\{Bi_2O_3^M \cdot Al_2O_3^N\}$ mixtures were studied using the HTXRD and DSC.

HTXRD was carried out stagewise. The initial mixture was studied by means of diffractometry at 25°C, heated to 400°C, and a spectrum was recorded; further spectra were measured at 400, 600, 730, 750, 780, and 805°C. In the course of cooling, pauses were made and spectra were measured at 780, 750, and 650°C.

According to the data obtained, starting from $T \geq$ 400°C, HTXRD registers the formation of low amounts of $Al_2Bi_{24}O_{39}$, $BiAlO_3$, and $Al_4Bi_2O_9$ phases formed according to reactions (5)–(7), which agrees well with the data of [8, 11]. Upon an increase in temperature, $Al_4Bi_2O_9$ becomes the main phase of the above complex intermediate phases.

However, the principal and most significant result is the following: the $\alpha \longrightarrow \delta$ transition of Bi_2O_3 occurs at $T \approx 730$°C in all equimolar $\{Al_2O_3^N \cdot Bi_2O_3^M\}$ mixtures prepared on the basis of any $Al_2O_3^N$ (Table 1).

Therefore, the sample at $T = 750$–805°C consists of δ-Bi_2O_3 and a relatively lower amount of $Al_4Bi_2O_9$. Thus, at any temperature the principal phase registered by XRD is one modification of Bi_2O_3. The XRD results for various temperatures are shown in Figs. 6a–6d and Table 2.

On the whole, the XRD data point to the high reactivity of $Al_2O_3^N$ towards $Bi_2O_3^M$: the formation of new phases occurs largely during the first heating to 805°C so that the phase composition is not changed as a result of further repeated cycling. It is for this reason that the shape of the temperature dependences of conductivity is preserved (Fig. 4).

The DSC data for the heating of the $\{Al_2O_3^N \cdot Bi_2O_3^M\}$ equimolar mixture are shown in Fig. 7. At ≈730°C, the endoeffect starts, which corresponds to the $\alpha \longrightarrow \delta$ transition of Bi_2O_3; at 783°C, another endoeffect starts that passes smoothly to the endoeffect at ≈790°C. The latter two effects are probably caused by transitions in the mixture of the complex composition and by the decomposition of Bi_2AlO_3 according to reaction (3). Let us note that, for most systems based on Bi_2O_3, metastable states and equilibriums are characteristic [15], complicating a precise interpretation of dynamic DSC data and their relationship with results obtained using other techniques. In this case there are grounds to assume that this is the cause for which the reaction (1) of the decomposition of $Al_2Bi_{24}O_{39}$, the primary product of interaction between Bi_2O_3 and Al_2O_3 [8, 11], does not appear on the DSC curve.

RESULTS AND DISCUSSION

Thus, in this work, a complex study of the processes occurring under heating in equimolar mixtures of microsized $Bi_2O_3^M$ and micro- and nanosized Al_2O_3 is performed. Let us summarize the key results:

(i) it was shown using the HTXRD and DSC techniques that the $\alpha \longrightarrow \delta$ polymorphic transition of Bi_2O_3 is registered in all mixtures at ≈730°C;

(ii) the temperature dependence of the $\sigma(T)$ dependence of the $\{Al_2O_3^M \cdot Bi_2O_3^M\}$ mixture practically coincides with the $\sigma(T)$ dependence of single-phase Bi_2O_3; in both cases, a 2.5-fold conductivity

Table 2. HTXRD data for the $\{Bi_2O_3^M \cdot Al_2O_3^N\}$ equimolar mixture

Exposure no.	Exposure temperature, °C	Sample history	Phase composition
1	25	Initial raw mixture of oxides	α-Bi_2O_3, $Al_2O_3^N$
2	780	1st heating	δ-Bi_2O_3, $Al_4Bi_2O_9$, $Al_2O_3^N$
3	25	First cycle after cooling from 805°C	α-Bi_2O_3, $Al_4Bi_2O_9$, $Al_2O_3^N$
4	25	After four successive "25 ⟶ 805 ⟶ 25°C" cycles	α-Bi_2O_3, $Al_4Bi_2O_9$, $Al_2O_3^N$

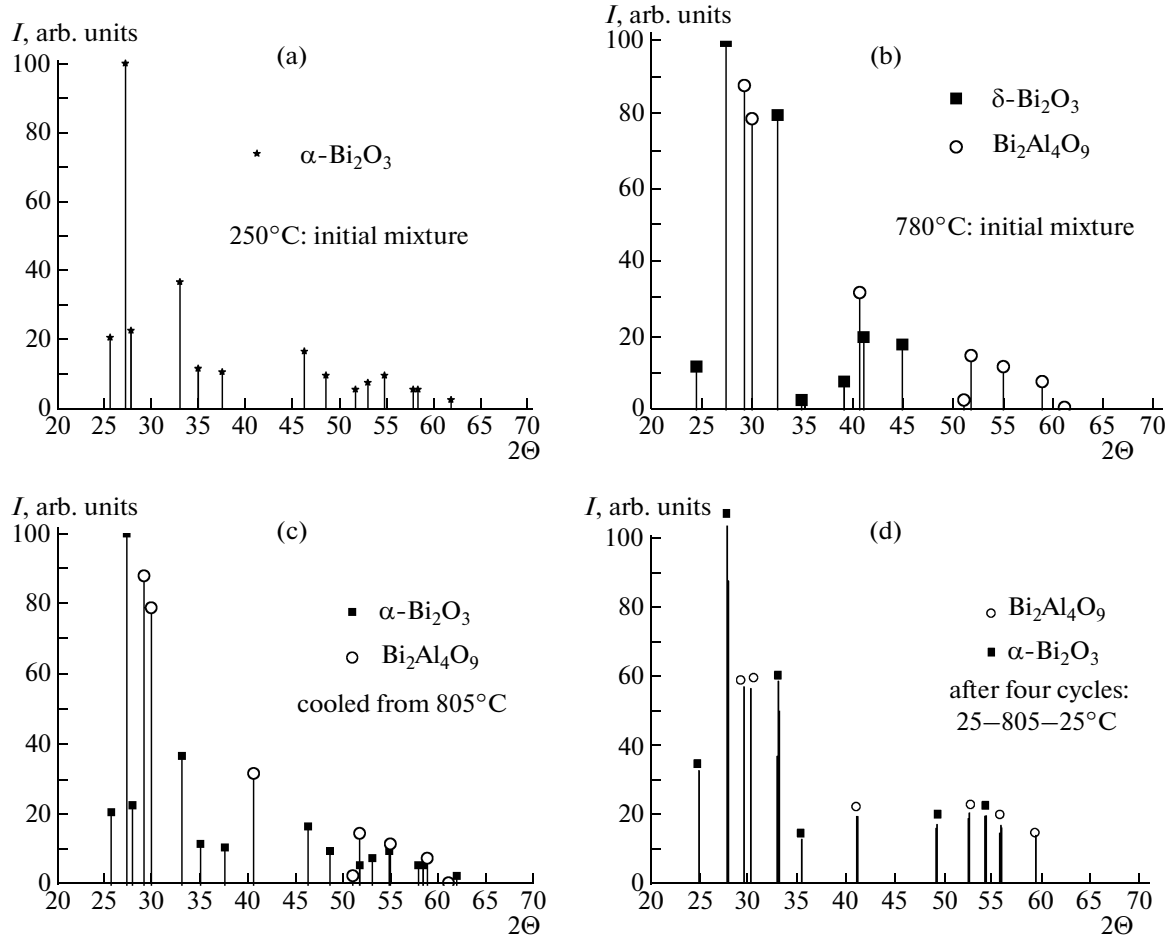

Fig. 6. HTXRD data of the $\{Al_2O_3^N \cdot Bi_2O_3^M\}$ mixture prepared on the basis of $Al_2O_3^N$ (S_{sp} = 97.5 m^2/g). See explanations in the text and in the figure.

jump is registered at ≈730°C due to the α ⟶ δ transition of Bi_2O_3;

(iii) in the case of the $\{Al_2O_3^N \cdot Bi_2O_3^M\}$ mixtures, a 2.5-fold conductivity jump is also observed, but there is no significant difference in its shape and range: there is no drastic σ jump at ≈730°C, only a slight inflection is observed, and the jump itself starts at 765 and ends at 800°C. For these mixtures, the σ(*T*) dependence further remains unchanged even after 10 successive 25 ⟶ 805 ⟶ 25°C cycles;

(iv) $Al_2O_3^N$ is characterized by high reactivity in the reaction with Bi_2O_3: the reaction largely ends during the first heating from 805°C, after which XRD detects the δ-Bi_2O_3 and $Al_4Bi_2O_9$ (805°C) or α-Bi_2O_3 and $Al_4Bi_2O_9$ (25°C) phases. The phase composition pattern does not change after several heating–cooling cycles or after additional sintering for 48 h at 750°C.

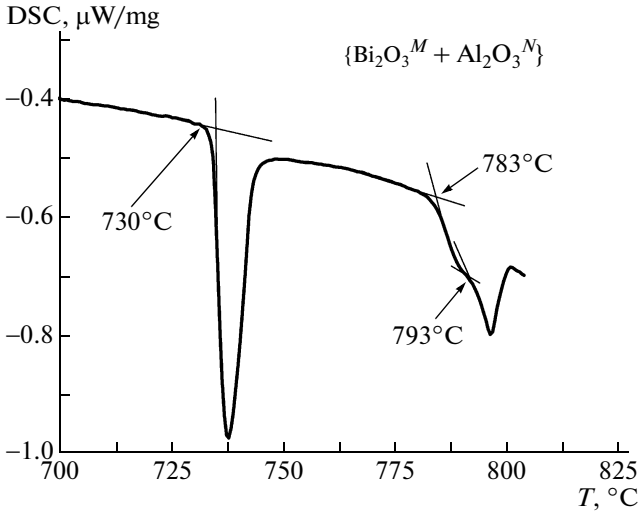

Fig. 7. DSC curve of heating of the $\{Al_2O_3^N \cdot Bi_2O_3^M\}$ mixture.

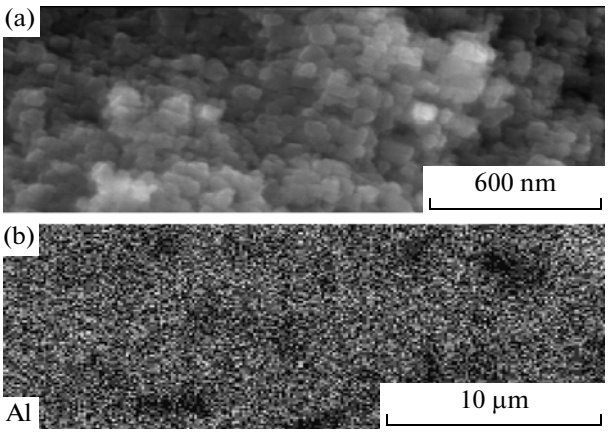

Fig. 8. SEM image of fracture of a briquette of the $\{Al_2O_3^N \cdot Bi_2O_3^M\}$ equimolar mixture after the first heating to 710°C: (a) direct image and (b) EDA image in back–scattered electrons.

The key problem is the issue of the reasons for the variation in the temperature range and the shape of the conductivity jump for the composite formed from the $\{Al_2O_3^N \cdot Bi_2O_3^M\}$ equimolar mixture as compared to single-phase Bi_2O_3 and the $\{Al_2O_3^M \cdot Bi_2O_3^M\}$ mixture. To answer this question, let us analyze the available experimental data on the chemistry and macromechanism of the interaction between $Bi_2O_3^M$ with nanosized $Al_2O_3^N$.

TEM studies showed that mixing $Bi_2O_3^M$ with $Al_2O_3^N$ and heating to 710°C results in the encapsulation of microsized Bi_2O_3 grains (≈8 μm) into a shell of nanograins of the $Al_2O_3^N$ oxide (20–40 nm) and interaction products (Figs. 8a, 8b).

A model experiment was carried out to test this hypothesis additionally: a sintered Bi_2O_3 briquette was placed into an $Al_2O_3^N$ charge and sintered for 10 h at 710°C. After sintering, a film of $Al_2O_3^N$ and interaction products was found on the surface of the Bi_2O_3 briquette (the TEM image is similar to that in Fig. 8). Such an observation contradicts the fact known from the literature of the higher coverage and mobility of Bi_2O_3 components in a reaction with Al_2O_3 (see above) and may be explained by the high energy of adhesion of $Al_2O_3^N$ grains to the surface of Bi_2O_3 grains.

Thus, in the case of heating, the internal part of the shell adjacent to Bi_2O_3 is transformed into a compact layer of low-conducting interaction products. The high density and adhesion of the $Al_2O_3^N$ layer and products to the Bi_2O_3 surface paralyze the known ability of Bi_2O_3 to quickly propagate over the surface and interface according to the mechanism of solid-phase spreading. Therefore, there is no direct contact between α-Bi_2O_3 grains (percolation network) and the low conductivity of the shell prevents the appearance of the α-δ-transition in the temperature dependences of conductivity.

Upon an increase in the temperature above 730°C (the point of α–δ-transition), chemical interaction is accelerated because the α ⟶ δ-Bi_2O_3 transition is already over and the reactivity and migration ability of δ-Bi_2O_3 is much higher [11]. It is important that the reaction occurs due to the outdiffusion of components of α-Bi_2O_3 from large grains of the Bi_2O_3 oxide to the external shell (such a diffusion pattern in terms of the kinetics of solid-phase reactions corresponds to the geometric model of "*anti*-Yander" [16]). Further, regularities of the thermodynamic phase stability of the Bi_2O_3–Al_2O_3 system within the shell isolating the δ-$Bi_2O_3^M$ grains begin to appear. At ≈755°C, the $Al_2Bi_{24}O_{39}$ phase is decomposed according to (1):

$$Al_2Bi_{24}O_{39} \longrightarrow 2BiAlO_3 + 11\delta\text{-}Bi_2O_3,$$

while at 780–800°C, solid–phase decomposition of $BiAlO_3$ occurs according to (2):

$$4BiAlO_3 \longrightarrow Al_4Bi_2O_9 + \delta\text{-}Bi_2O_3.$$

As may be seen, decomposition reactions (6) and (7) result in the appearance of the δ-Bi_2O_3 phase inside a shell that has earlier briquetteed direct contact between Bi_2O_3 grains. As a result, a continuous connected conducting matrix of δ-Bi_2O_3 grains is formed (probably, δ-$Bi_2O_3^N$) and, at a temperature of about 765–800°C, a 2.5-fold increase in conductivity is observed, as follows from the corresponding difference in conductivity of δ- and α-Bi_2O_3.

In the case of cooling, reactions (1) and (2) are reversed and the cooling curves feature a drastic decrease in conductivity due to the regeneration of an isolating shell around the α-Bi_2O_3 grains.

This model was tested by experimentally measuring the temperature dependence of conductivity of briquette assemblies simulating the structure and processes in a shell encapsulating $Bi_2O_3^M$ grains. Model experiments were performed for the following briquette assemblies:

$$|Bi_2O_3| \text{ thin layer of } \underset{Al_2O_3^N}{} |Bi_2O_3|, \quad (7)$$

$$|Bi_2O_3|Al_2Bi_{24}O_{39}|BiAlO_3|, \quad (8)$$

$$|Bi_2O_3|BiAlO_3|, \quad (9)$$

$$|Bi_2O_3|Al_2Bi_{24}O_{39}|. \quad (10)$$

It turned out that the $\sigma(T)$ dependences for all assemblies (7)–(10) feature a conductivity jump in the range of 760–800°C and the shape of the dependences

is quite similar to the studied $\sigma(T)$ dependence of the $\{Al_2O_3^N \cdot Bi_2O_3^M\}$ briquette mixture (Figs. 3, 4). It is important that the $\sigma(T)$ data for (7)–(10) made it possible to specify the fine details of this dependence, in particular, to separately observe an increase in conductivity due to processes (1) and (2).

Proof of the above model is the presence of threshold values of fractional concentration $\varphi_{Al_2O_3} = [Al_2O_3^N]/[Bi_2O_3^M] + [Al_2O_3^N]$, at which a fundamental change occurs in the shape of the $\sigma(T)$ dependence, including the screening of the α–δ-transition of Bi_2O_3 due to the encapsulation effect. For this purpose, the $\sigma(T)$ dependences were measured for briquette mixtures prepared at the step of $\varphi_{Al_2O_3} = 0.1$. This experiment showed the presence of three concentration ranges:

(1) $\varphi_{Al_2O_3} > 0.80$: the $\sigma(T)$ dependence is close to the dependence for $Al_2O_3^N$ (Fig. 2) and the conductivity jump is absent;

(2) $0.80 < \varphi_{Al_2O_3} > 0.20$: this corresponds to the concentration range of encapsulation of $Bi_2O_3^M$ grains, in which the $\sigma(T)$ dependence features an extended conductivity jump (Figs. 3, 4) and the percolation system formed by δ-Bi_2O_3 is formed above 765°C;

(3) $\varphi_{Al_2O_3} < 0.20$: the $\sigma(T)$ dependence is close to that of $Bi_2O_3^M$ (Fig. 2) and the conductivity jump occurs at 730°C; i.e., there is a continuous conducting matrix of $Bi_2O_3^M$ grains in the composites.

CONCLUSIONS

A complex of modern instrumental and model methods showed the fundamental differences in the mechanisms of the processes accompanying the interaction between nano- and microsized Al_2O_3 with Bi_2O_3 and routes of charge transfer in the composite generated as a result of their interaction.

The main reason for the observed differences is the size effect manifested in the form of the strong adhesion of $Al_2O_3^N$ grains to the surface of microsized $Bi_2O_3^M$ grains and the high reactivity of $Al_2O_3^N$. Both factors result in the encapsulation of $Bi_2O_3^M$ grains in a shell of low-conducting $Al_2O_3^N$ grains and interaction products. During the first cycling of the $\{Al_2O_3^N \cdot Bi_2O_3^M\}$ equimolar mixture to the temperature below 730°C, interaction products, phase composition (α-Bi_2O_3 and Al–Bi oxide phases), and composite morphology are formed. Herewith, the rarely observed anti-Yander reaction diffusion geometry is implemented: the mass transport of mobile components from a $Bi_2O_3^M$ large grain out to $Al_2O_3^N$ through a layer of products.

Therefore, the phase transition of α ⟶ δ-Bi_2O_3 occurs inside mutually isolated $Bi_2O_3^M$ grains at 730°C and is registered using the HTXRD and DSC techniques but does not appear in the temperature dependence of conductivity. Further heating up to 780°C results in the solid–phase decomposition of interaction products and the separation of the δ-Bi_2O_3 phase inside the shell surrounding $Bi_2O_3^M$ grains. Lastly, a connected matrix is formed of highly conducting δ-Bi_2O_3 grains. Owing to this, a 2.5-fold conductivity jump is observed in the range of 780–805°C due to an increase in the amount of the δ-Bi_2O_3 phase.

The above scenario of reaction evolution and charge transfer routes were confirmed by measurements of $\sigma(T)$ dependences for four cells simulating the composition, structure, and reactions at various stages of process development.

Important additional proof of the above pattern was the presence of three concentration ranges of the $[Al_2O_3^N]/[Bi_2O_3^M]$ ratio with different forms and temperatures of their conductivity jumps in the $\sigma(T)$ dependences.

The observed regularities demonstrate unusual characteristics for the reactivity of nanooxides and the mechanism of processes with their participation. The obtained results are important, because processes of such a nature may occur during the synthesis of high-temperature nanocomposite materials, distributed materials with metal, or semiconductor nanoclusters dispersed in a dielectric matrix [1, 2] and may fundamentally affect the functional properties of materials.

ACKNOWLEDGMENTS

We are sincerely grateful to Yu.A. Kotov (Institute of Electrophysics, Ural Division, Russian Academy of Sciences) for the $Al_2O_3^N$ samples and data on their morphology, as well as for supporting this work and helpful discussions, and to L.A. Isupova (Institute of Catalysis, Siberian Division, Russian Academy of Sciences) for making pseudoboehmite available and N.N. Pestereva (Ural State University) for her help in processing the results and preparing the manuscript.

REFERENCES

1. G. B. Sergeev, "Size Effects in Nanochemistry," Ross. Khim. Zh. **XLVI** (5), 22–29 (2002).

2. N. F. Uvarov and V. V. Boldyrev, "Size Effects in Chemistry of Heterogeneous Systems," Usp. Khim. **70** (4), 307–329 (2001).
3. J. Maier, "Thermodynamic Aspects and Morphology of Nano-Structured Ion Conductors: Aspects of Nano-Ionics: Part I," Solid State Ionics **154–155**, 291 (2002).
4. A. Ya. Neiman, "Cooperative Transport in Oxides: Diffusion and Migration Processes Involving Mo(VI), W(VI), V(V), and Nb(V)," Solid State Ionics **83**, 263–273 (1996).
5. A. Ya. Neiman, N. N. Pestereva, A. R. Sharafutdinov, and Yu. P. Kostikov, "Conduction and Transport Numbers in Metacomposites $MeWO_4 \cdot WO_3$ (Me = Ca, Sr, Ba)," Elektrokhimiya **41** (6), 680–693 (2005) [Russ. J. Electrochem. **41** (6), 598–611 (2005)].
6. A. Ya. Neiman, N. F. Uvarov, and N. N. Pestereva, "Solid State Surface and Interface Spreading: An Experimental Study," Solid State Ionics **177**, 3361–3369 (2007).
7. A. Neiman, E. Tsipis, I. Beketov, Yu. Kotov, A. Murzakaiev, and O. Samatov, "Solid State Interactions in Nanosized Oxides," Solid State Ionics **177**, 403–410 (2006).
8. Yu. F. Kargin, V. I. Burkov, A. A. Mar'in, and A. V. Egorysheva, *Crystals $Bi_{12}M_xO_{20\pm\delta}$ with the Sillenite Structure: Synthesis, Structure, and Properties* (Azbuka, Moscow, 2004) [in Russian].
9. *Phase Diagrams of the Refractory Oxide Systems: A Handbook*, Issue 5: *Binary Systems*, Ed. by F. Ya. Galakhov (Nauka, Leningrad, 1986), Part 2, p. 286 [in Russian].
10. H. Knozinger and E. Taglauer, "Toward Supported Oxide Catalysts via Solid–Solid Wetting," Catalysis **10**, 1–40 (1993).
11. T. B. Belkova, E. G. Vovkotrub, and A. Ya. Neiman, "Macromechanism of Solid-State Reactions of Bi_2O_3 with Oxides of Aluminum and Rare-Earth Metals," Zh. Neorg. Khim. **39** (2), 219–222 (1994).
12. *Solid Electrolytes*, Ed. by S. Geller, in *Topics in Applied Physics* (Springer, Berlin, 1997), Vol. 21.
13. *Solid State Electrochemistry*, Ed. by P. G. Bruce (Cambridge University Press, Cambridge, 1997).
14. Yu. A. Kotov, A. V. Bagazeev, A. I. Medvedev, A. M. Murzakaev, T. M. Demina, and A. K. Shtolts, "Characteristics of Aluminum Oxide Nanopowders Produced by Electric Explosion of Wire," Ross. Nanotekhnol. **2** (7–8), 109–115 (2007).
15. V. M. Skorikov and Yu. F. Kargin, in *Chemistry of Bismuth Oxide Compounds: Investigations into Inorganic Chemistry and Chemical Technology* (A Collection of Scientific Works) (Institute of General and Inorganic Chemistry of the Academy of Sciences of the Soviet Union, Moscow, 1988), pp. 261–304 [in Russian].
16. Yu. D. Tret'yakov, *Solid-Phase Reactions* (Khimiya, Moscow, 1978) [in Russian].